Monte Carlo methods for turbulent tracers with long range and fractal random velocity fields

Frank W. Elliott, Jr., David J. Horntrop, and Andrew J. Majda
Courant Institute of Mathematical Sciences, 251 Mercer Street, New York, New York 10012

(Received 31 May 1996; accepted for publication 8 August 1996)

Monte Carlo methods for computing various statistical aspects of turbulent diffusion with long range correlated and even fractal random velocity fields are described here. A simple explicit exactly solvable model with complex regimes of scaling behavior including trapping, subdiffusion, and superdiffusion is utilized to compare and contrast the capabilities of conventional Monte Carlo procedures such as the Fourier method and the moving average method; explicit numerical examples are presented which demonstrate the poor convergence of these conventional methods in various regimes with long range velocity correlations. A new method for computing fractal random fields involving wavelets and random plane waves developed recently by two of the authors [J. Comput. Phys. **117**, 146 (1995)] is applied to compute pair dispersion over many decades for systematic families of anisotropic fractal velocity fields with the Kolmogorov spectrum. The important associated preconstant for pair dispersion in the Richardson law in these anisotropic settings is compared with the one obtained over many decades recently by two of the authors [Phys. Fluids **8**, 1052 (1996)] for an isotropic fractal field with the Kolmogorov spectrum. © *1997 American Institute of Physics.* [S1054-1500(97)01001-X]

Fractal random fields arise in a wide variety of physical problems including flow through porous media, turbulent diffusion in the environment, and topography in statistical physics. One important means of studying such problems is through computer simulations using Monte Carlo techniques. In this paper, we concentrate on the statistics of tracers. We begin by validating two well-known Monte Carlo simulation techniques (the Fourier method and the moving average method) using an unambiguous, exactly solvable, yet nontrivial model problem with long range correlations, thereby demonstrating many of the pitfalls associated with the use of these methods. Finally, we consider a new wavelet-based simulation technique which has been shown elsewhere [J. Comput. Phys. 113, 82 (1994)] not to display any of the spurious behavior seen above; this technique is used in a study of the relative spreading of pairs of particles for a family of anisotropic velocity fields and a comparison is made with earlier results for the spreading of pairs of particles under the influence of an isotropic velocity field [Phys. Fluids 8, 1052 (1996)].

I. INTRODUCTION

Generating random velocity fields, $\mathbf{v}(\mathbf{x},t)$, with long range correlations in space and/or time is an important practical issue in diverse applications ranging from flow in porous media,[1] turbulent diffusion in environmental applications,[2,3] and random topography in statistical physics.[4,5] The challenge is to develop algorithms which are accurate and efficient over a wide scaling range so that these methods can be used with confidence to predict various important scaling laws in physics such as Richardson's t^3 law for the dispersion of pairs of particles.[2] Here we describe various numerical algorithms including standard ones such as the Fourier method and the moving average method as well as novel methods for fractal random fields which have been developed recently by the authors.[6,7] We also describe the application of these algorithms to tracer statistics.

The simplest tracer statistic of the sort used here measures the spreading of particles from a fixed source. We assume for simplicity that the velocity field $\mathbf{v}(\mathbf{x},t)$ has zero mean, i.e., $\langle \mathbf{v}(\mathbf{x},t)\rangle = 0$, where, here and below, $\langle\cdot\rangle$ denotes ensemble average over the velocity statistics. We consider solutions of the nonlinear ordinary differential equation

$$\frac{d\mathbf{X}}{dt} = \mathbf{v}(\mathbf{X},t),$$
$$\mathbf{X}(0) = \mathbf{X}_0. \tag{1}$$

Then, the mean square displacement in the ith direction is given by

$$\langle |X_i|^2(t)\rangle, \quad 1 \leqslant i \leqslant d. \tag{2}$$

For stationary random fields which have translation invariant statistics, the number in (2) does not depend of the initial location $\mathbf{X}_0$; for simplicity in exposition, we assume stationary random velocity fields throughout this paper. Ordinary diffusion occurs when the mean square displacement scales like

$$\langle |X_i|^2(t)\rangle \sim D_i^* t \tag{3}$$

for large times, $t \gg 1$, with $D_i^* > 0$, the diffusion coefficient in the ith direction. Recently, many applications in statistical physics[1–3] reveal anomalous diffusion where the scaling in (3) is replaced by

$$\langle |X_i|^2(t)\rangle \sim D_i^* t^{\alpha} \tag{4}$$

for large times, $t \gg 1$, where either $0 \leq \alpha < 1$, subdiffusive, or $\alpha > 1$, superdiffusive.

In Sec. II of this paper we present the simplest elementary exactly solvable model demonstrating both subdiffusion and superdiffusion. Such simple models with complex behavior provide ideal candidates for evaluating the capability of Monte Carlo methods to compute the correct scaling behavior. Such elementary models can also be used to display inherent numerical artifacts in conventional numerical methods. Examples of this sort utilizing the conventional Fourier method and the moving average method are presented in Sec. II.

Another statistical quantity that is very important in turbulent diffusion occurs for pair separation statistics. We begin with two particles, $\mathbf{X}_j$, for $j=1,2$ with fixed initial separation distances, s, so that

$$|\mathbf{X}_1(0)-\mathbf{X}_2(0)|=s \tag{5}$$

and follow the pair separation

$$\mathbf{X}_1(t)-\mathbf{X}_2(t),$$

where each particle moves separately according to the nonlinear ordinary differential equation in (1). The pair separation at later times, $\mathbf{X}_1(t)-\mathbf{X}_2(t)$, is a stationary random variable depending on the velocity statistics; the pair dispersion, $\sigma^2(t,s)$, is the second moment of this random variable,

$$\langle |\mathbf{X}_1(t)-\mathbf{X}_2(t)|^2 \rangle = \sigma^2(t,s). \tag{6}$$

When the velocity field $\mathbf{v}(\mathbf{x},t)$ is a fractal random field with the Kolmogorov spectrum, there are famous experimental and theoretical predictions[2,8,9] that reveal the behavior

$$\sigma^2(t,s) \cong G_\Delta t^3 \tag{7}$$

for large times, $t \gg 1$. The constant G_Δ does not depend on the initial separation and is supposed to be universal with appropriate nondimensionalization of the velocity field. The scaling behavior in (6) is known as Richardson's law[8] and there is great interest in obtaining both the scaling law and the constant G_Δ accurately as a function of the fractal velocity field, $\mathbf{v}(\mathbf{x},t)$.

In Sec. III, we apply the new method for computing fractal random fields involving wavelets and random plane waves[6,7,10] to calculating pair dispersion over many scaling decades for systematic families of anisotropic fractal velocity fields with the Kolmogorov spectrum. These new results both confirm Richardson's law in this anisotropic setting over many scaling decades and also give a preconstant G_Δ over many decades with a value very similar to the one obtained recently by two of the authors[10] for isotropic velocity fields.

II. SIMPLE EXACT MODELS WITH ANOMALOUS DIFFUSION AND NUMERICAL TEST PROBLEMS FOR MONTE CARLO METHODS

The simplest models which are exactly solvable and reveal anomalous scaling behavior[11] involve simple shear layer flows with the velocity field $\mathbf{v}(\mathbf{x},t)$ given by

$$\mathbf{v}(\mathbf{x},t)=\begin{pmatrix} \overline{w} \\ v(x) \end{pmatrix}, \tag{8}$$

where $\overline{w}$ is a fixed constant and $v(x)$ is a zero mean, Gaussian random field. Gaussian random velocity fields, $v(x)$, are completely characterized by the two-point correlation function, $\langle v(x+x')v(x') \rangle = R(x)$, which admits the Fourier representation

$$\langle v(x+x')v(x') \rangle = R(x) = \int_{-\infty}^{\infty} \cos(kx) S(k)\, dk, \tag{9}$$

where $S(k)$ is the spectral energy density of the random field $v(x)$. Here we use the notation $\mathbf{x}=(x,y)$ for the coordinates in two dimensions. Thus, the fluid flow in (8) represents a constant mean flow along the x axis and random shearing along the y axis defined by the field $v(x)$. Following the pioneering efforts of Matheron and de Marsily,[12] many researchers[13–17] have utilized such simple shear layer models in steady and time-dependent settings often with $\overline{w}=0$ and nonzero molecular diffusion to illustrate several remarkable aspects of anomalous diffusion. The calculation described here with $\overline{w} \neq 0$ yields anomalous scaling behavior in a completely elementary fashion.

A. Anomalous scaling for mean square displacements

Consider the spreading of particles from the origin (0,0). The solution of the particle trajectory equation from (1) for the special velocity field in (8) is given by

$$\begin{aligned} X(t) &= \overline{w}t, \\ Y(t) &= \int_0^t v(\overline{w}s)\, ds. \end{aligned} \tag{10}$$

With (10), the mean square displacement in the y direction is given by

$$\langle Y^2(t) \rangle = \left\langle \int_0^t v(\overline{w}s)\, ds \int_0^t v(\overline{w}s')\, ds' \right\rangle. \tag{11}$$

By interchanging the order of integration and using the Fourier representation for the covariance, $R(x)$, from (9), we obtain the formulas

$$\begin{aligned} \langle Y^2(t) \rangle &= \int_0^t \int_0^t \langle v(\overline{w}s) v(\overline{w}s') \rangle ds'\, ds \\ &= \int_0^t \int_0^t R(\overline{w}|s-s'|) ds'\, ds \\ &= \frac{4}{\overline{w}^2} \int_0^\infty [1-\cos(k\overline{w}t)] \frac{S(|k|)}{|k|^2}\, dk. \end{aligned} \tag{12}$$

The second equality in (12) demonstrates that for these simple models the mean square displacement is completely determined by the covariance $R(x)$.

To obtain a rich family of velocity fields with a wide variety of scaling behavior, we consider random velocity fields with the parametrized family of velocity spectra given explicitly by

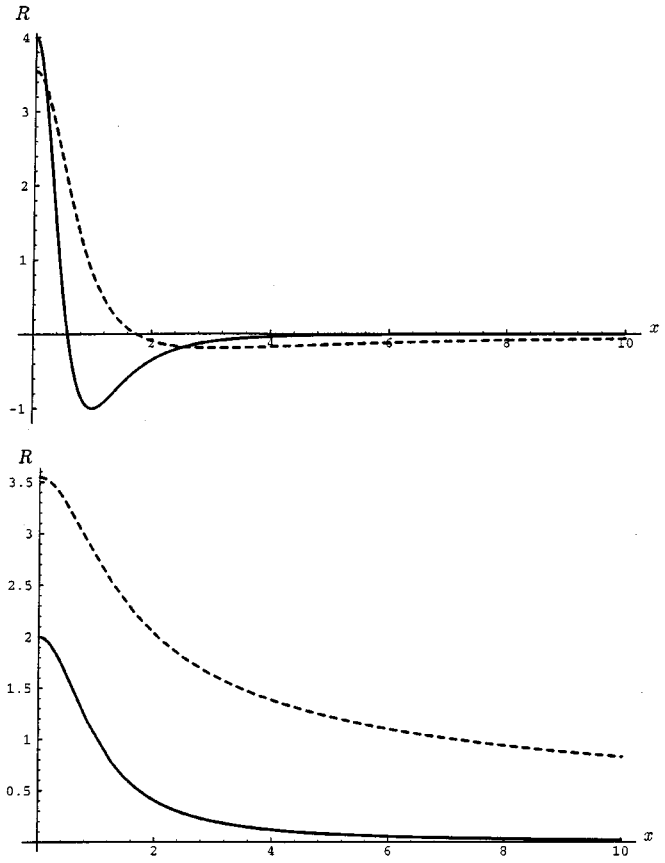

FIG. 1. The effect of adjusting ϵ on the covariance function. The top plot demonstrates the long ranges of negative correlation for $\epsilon=-1$ (solid line) and $\epsilon=\frac{1}{2}$ (dashed line). The bottom plot shows the increase in long range correlation between $\epsilon=1$ (solid line) and $\epsilon=\frac{3}{2}$ (dashed line).

$$S_{\epsilon,\alpha}(k)=|k|^{1-\epsilon}e^{-\alpha|k|}, \quad -\infty<\epsilon<2. \tag{13}$$

For this family of spectra in (13), the covariance is calculated explicitly to be given by

$$R(x)=2\Gamma(2-\epsilon)(\alpha^2+x^2)^{\epsilon/2-1}\cos\left((2-\epsilon)\arctan\left(\frac{|x|}{\alpha}\right)\right). \tag{14}$$

For certain values of ϵ, the results in (14) have an even simpler form; for example, for $\epsilon=1$ we have

$$R(x)=\frac{2\alpha}{\alpha^2+x^2}. \tag{15}$$

A remarkably wide variety of behavior occurs for the covariance function $R(x)$ as the spectral parameter ϵ is varied for $\epsilon<2$. Figure 1 depicts this covariance function for $\alpha=1$ and $\epsilon=-1$, $\frac{1}{2}$, 1, $\frac{3}{2}$. The cases with $\epsilon=-1$, $\frac{1}{2}$ have an oscillatory tail so that there are large regions of negative correlation for the velocity field. For $\epsilon\geqslant 1$, the tail of the covariance no longer oscillates; however, for larger ϵ, the tail of the covariance decays much more slowly, indicating that longer range correlations in the velocity field occur in this regime.

For these specific random velocity fields defined in (9) and (13), the mean square displacement can be calculated explicitly for all times. For $\epsilon\neq 0$, 1 and $\epsilon<2$, we have

$$\langle Y^2(t)\rangle=\frac{4\Gamma(-\epsilon)}{\overline{w^2}}\left[\alpha^{\epsilon}-(\alpha^2+(\overline{wt})^2)^{\epsilon/2}\times\cos\left(\epsilon\arctan\left(\frac{\overline{wt}}{\alpha}\right)\right)\right], \tag{16}$$

while for $\epsilon=0$

$$\langle Y^2(t)\rangle=\frac{2}{\overline{w^2}}\ln\left(1+\frac{\overline{w^2}t^2}{\alpha^2}\right), \tag{17}$$

and for $\epsilon=1$

$$\langle Y^2(t)\rangle=\frac{4}{\overline{w^2}}\left[|\overline{wt}|\arctan\left(\frac{|\overline{wt}|}{\alpha}\right)-2\alpha\ln\left(1+\frac{\overline{w^2}t^2}{\alpha^2}\right)\right]. \tag{18}$$

From these explicit formulas, it is a simple matter to compute the large time scaling behavior for the mean square displacements as ϵ is varied which we summarize in Table I. Note the logarithmic behavior in the mean square displacement for $\epsilon=0$. Thus, this elementary example exhibits complex behavior in the mean square displacement ranging from trapping for $\epsilon<0$ to subdiffusion for $0\leqslant\epsilon<1$ to superdiffusion for $1<\epsilon<2$. The effect of molecular diffusion in these models also has been computed,[11] and the regimes with trapping and subdiffusion for $\epsilon<1$ are replaced by diffusive scaling.

What creates the diffusion of mean square displacements in y for $0<\epsilon<2$ as compared with the trapping behavior for $\epsilon<0$? Formally, solutions of (1) with the special velocity field in (8) stay on the zero level set of the stream function $\Psi(x,y)$ where

$$\Psi(x,y)=\overline{wy}-\psi(x)$$

with

$$\psi(x)=\int_0^x v(x')dx'. \tag{19}$$

Thus, the streamline through (0,0) for each realization is given by the graph

$$y=\frac{1}{\overline{w}}\psi(x), \tag{20}$$

where the average value of $\psi(x)$ can be computed from (19), (20), (8), and (9) as given formally by

$$\langle|\psi^2(y)|\rangle=\int_0^{\infty}|k|^{1-\epsilon}e^{-\alpha|k|}\,dk. \tag{21}$$

For $\epsilon<0$, we have $\langle|\psi^2|\rangle<\infty$, streamlines in y remain bounded, and with (20) and (21), trapping occurs. On the other hand, for $0<\epsilon<2$, $\langle|\psi^2|\rangle=+\infty$ and the streamlines are typically unbounded in y, yielding nontrivial growth in y; furthermore, from (21), this growth increases as ϵ increases for $0<\epsilon<2$. In fact, the reader can easily verify that the graph of this streamline at large scales behaves like the graph of a fractal random field with Hurst exponent $\epsilon/2$ for $0<\epsilon<2$.

The wide variety of behavior of the mean square displacements as ϵ is varied together with the explicit formulas

TABLE I. Summary of the large scale, long time behavior for the mean square displacement when $\overline{w}\neq 0$ for the simple shear layer model introduced in (8), (9), and (13).

Parameter regime	Mean square displacement	Qualitative behavior
$\epsilon<0$	$\langle Y^2(t)\rangle \sim t^0$	trapping
$0<\epsilon<1$	$\langle Y^2(t)\rangle \sim t^\epsilon$	subdiffusive
$\epsilon=1$	$\langle Y^2(t)\rangle \sim t$	diffusive
$1<\epsilon<2$	$\langle Y^2(t)\rangle \sim t^\epsilon$	superdiffusive

in (16)–(18) provide an unambiguous family of elementary test problems for Monte Carlo methods with rich behavior.

B. The Fourier method for Monte Carlo simulation

The starting point for the Fourier method is the representation of the Gaussian random field with the energy density, $S(k)$, from (9) as a stochastic Fourier integral with respect to white noise,

$$v(x)=\int_{-\infty}^{\infty} e^{ikx}S^{1/2}(k)dW(k), \tag{22}$$

where $dW(k)$ is complex Gaussian white noise satisfying

$$\langle dW(k)dW(k')\rangle=\delta(k+k')dkdk'. \tag{23}$$

Fourier methods involve a midpoint rule discretization of (22), yielding the approximation

$$v_a(x)=\sum_{i=0}^{M} a_i\cos(k_i x)+b_i\sin(k_i x), \tag{24}$$

where a_i, b_i are independent identically distributed Gaussian random variables with mean zero and variance $S(k_i)\Delta k_i$, i.e., $\langle a_i^2\rangle=\langle b_i^2\rangle=S(k_i)\Delta k_i$. In the standard Fourier methods,[18] the wave number grid points, k_i, are chosen deterministically and are equally spaced in order to utilize the fast Fourier transform for the rapid evaluation of (24); thus $\Delta k_i=\Delta k$ for $i=1,\ldots,M$, $\Delta k_0=\Delta k/2$, and $k_i=i\Delta k$.

The first thing to notice about the Fourier method is that

every realization, v_a,

is periodic with period $2\pi/\Delta k$

even though the original random field $v(x)$

in (22) is not necessarily periodic. (25)

How serious are these finite periodicity effects in the practical use of the Fourier method for turbulent tracer statistics?

To demonstrate these effects, we consider the Monte Carlo simulation of the mean square displacement, $\langle Y^2(t)\rangle$, for the spectrum with the value $\epsilon=\frac{1}{2}$ and $\alpha=1$ in (13). Here and below we utilized the normalization $\overline{w}=1$. We selected a largest wave number $k_{\max}=10$ guaranteeing that less than 0.1% of the energy density of the original field was not represented in the finite truncation in (24). We picked a fine wave number spacing $\Delta k=0.05$ and time integration via the trapezoidal method with $\Delta t=0.1$. For these parameters, the numerical period from (25) of the Fourier method is roughly 125 and each realization utilizes 400 random Fourier modes. The Monte Carlo simulation of $\langle Y^2(t)\rangle$ with this Fourier algorithm ensemble averaged over 2000 realization is depicted in Fig. 2 and compared with the exact formulas from (16). The periodicity effects are quite remarkable; even by a time $t\cong 15$, which is roughly $\frac{1}{8}$ the period of the simulation (recall that spatial and temporal discretization are comparable), the downward trend in the numerical solution is quite noticeable. We reduced Δk by a factor of 4 to $\Delta k=0.0125$ and this increased the artificial period of the Fourier method to roughly 500 and kept all other parameters in the Monte Carlo method fixed. The comparison with the exact solution and the Fourier method with 2000 realizations given in Fig. 3 indicates that the mean square displacement is computed accurately to the modest time of roughly 60 shown there, the expected fourfold improvement in time from periodicity effects. This resulting improvement demonstrates explicitly that the large error in Fig. 2 is caused by finite periodicity effects rather than truncation and discretization errors. However, even the simulation in Fig. 3, which is accurate for comparatively short times, involves 1600 Fourier modes in each realization and exhibits strong downward trends after the time depicted in Fig. 3.

The above examples demonstrate in unambiguous fashion the failure of the conventional equispaced Fourier method in computing simple statistics of a turbulent tracer. There are other variants of the Fourier method[19,20] which rely upon nonequispaced random quadrature points where such finite periodicity effects are minimized; of course, such Fourier methods no longer have a fast Fourier transform associated with them.

C. The moving average method for Monte Carlo simulation

The starting point for the moving average method is the physical space representation

$$v(x)=\int_{-\infty}^{\infty} G(x'-x)dW(x')=\int_{-\infty}^{\infty} G(x')dW(x'+x), \tag{26}$$

where $W(x')$ is the Weiner process and the function $G(x)$ is the Fourier transform of the square root of the energy spectrum $S(k)$,

$$G(x)=2\int_0^{\infty}\cos(2\pi kx)S^{1/2}(k)dk. \tag{27}$$

The moving average method involves a simple discretization of (26), resulting in the approximation

$$v_a(x)=\sum_{i=-p}^{p} G(r_i)Z(r_i+x), \tag{28}$$

where Z is a Gaussian random variable with mean zero and variance Δr_i; the grid points r_i are chosen to be equally spaced, making $\Delta r_i=\Delta r$.

How well does the approximate random field in (28) compare with the true random field $v(x)$? Since both are Gaussian random fields with $\langle v(x)\rangle=\langle v_a(x)\rangle=0$, the im-

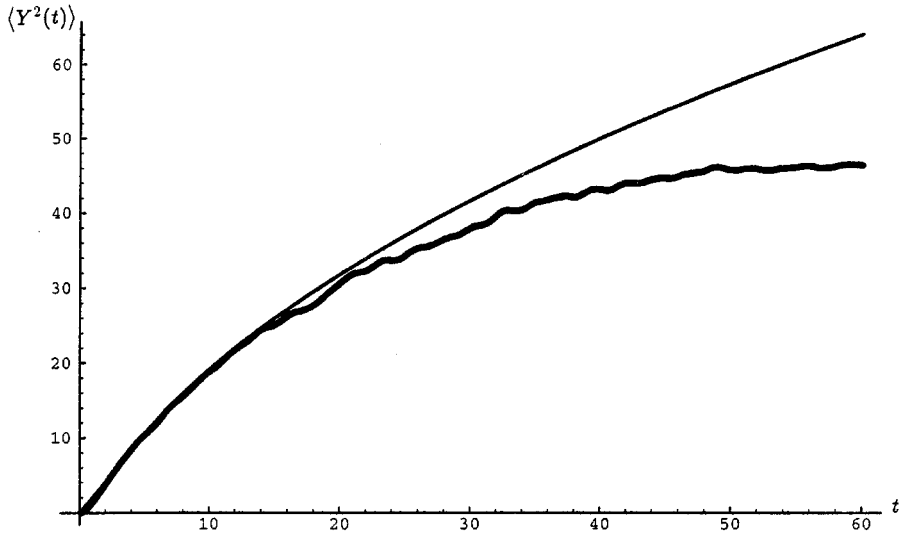

FIG. 2. Fourier method mean square displacement simulation results for $\epsilon=\frac{1}{2}$ (thicker line) versus the true value from (16) (thinner line). Even though the period of the simulated field is about 125, the periodicity effects are already evident by time 15.

portant quantity to check is the accuracy of the approximate covariance function. If we require that $x=j\Delta r$ with $j<2p$, i.e., $x<2p\Delta r=r_{\max}$, then we have the following explicit formula for the approximate covariance from the moving average method;

$$R_a(x)=\langle v_a(x'+x)v_a(x')\rangle=\sum_{i=-p+j}^{p} G(r_i)G(r_{i-j})\Delta r \tag{29}$$

and $R_a(x)\equiv 0$ for $j\geqslant 2p$. On the other hand, from (9) and (27) we obtain that the exact covariance $R(x)$ is given by

$$R(x)=\langle v(x'+x)v(x')\rangle=\int_{-\infty}^{\infty} G(r)G(r-x)dr. \tag{30}$$

Thus, the approximate covariance with the moving average method from (29) is a trapezoidal quadrature approximation of the covariance representation from (30) for the exact random field $v(x)$. We remark here that for spectra $S(k)$ of the form in (13) we have explicit formulas for the function $G(x)$ in (27) and (29) simply because $(S_{\epsilon,\alpha}(k))^{1/2}=S_{\epsilon/2+1/2,\alpha/2}(k)$ and the same general formulas from (14) apply.

We report on Monte Carlo simulations with the moving average method in the superdiffusive regime with $\epsilon=\frac{3}{2}$ where the velocity field has significant long range correlations. First, in Figs. 4 and 5 we plot the exact covariance from (29) generated by the moving average method with the two parameter values $r_{\max}=80$ and 160, respectively, and $\Delta r=0.1$. The corresponding value of the bandwidth p in (28) is 800

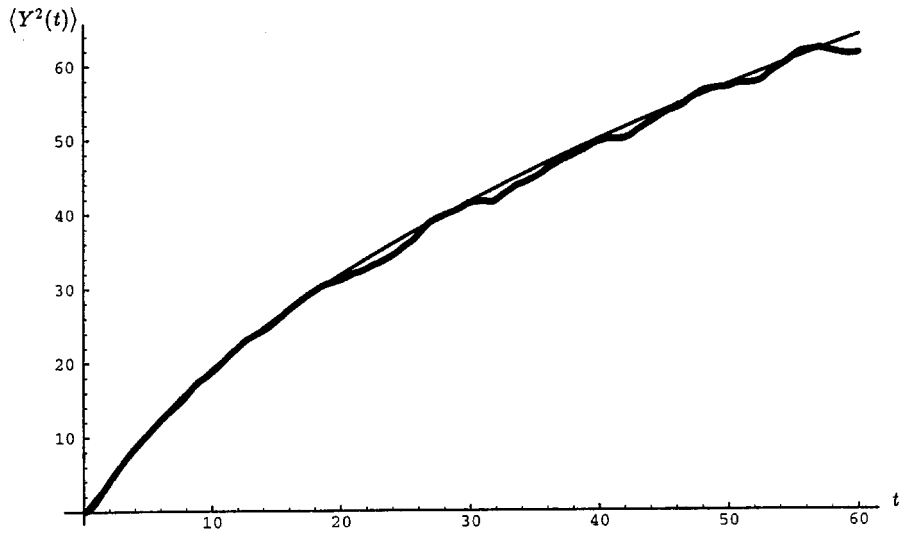

FIG. 3. Fourier method mean square displacement simulation results for $\epsilon=\frac{1}{2}$ (thicker line) versus the true value from (16) (thinner line). The period of the simulated field is increased by a factor of 4 when compared with Fig. 2 to the value 500, thereby eliminating the periodicity effects on the results to the modest time 60.

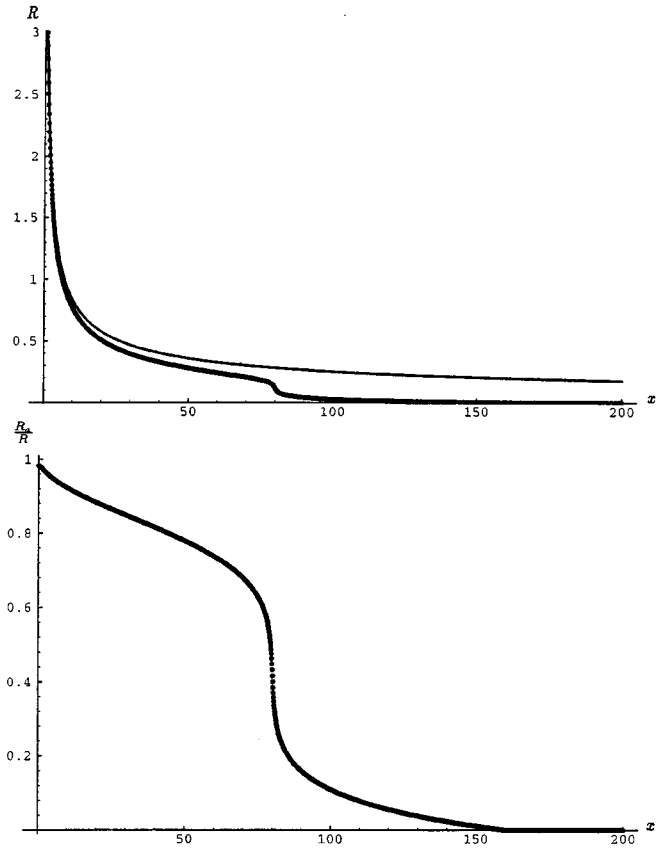

FIG. 4. The top plot contains a comparison of the true covariance function from (14) (thinner line) with the moving average method covariance function from (29) (thicker line) for $\epsilon=\frac{3}{2}$ and $r_{\max}=80$. The bottom plot is the ratio of these two quantities showing explicitly the fraction of the covariance reproducible by the moving average method.

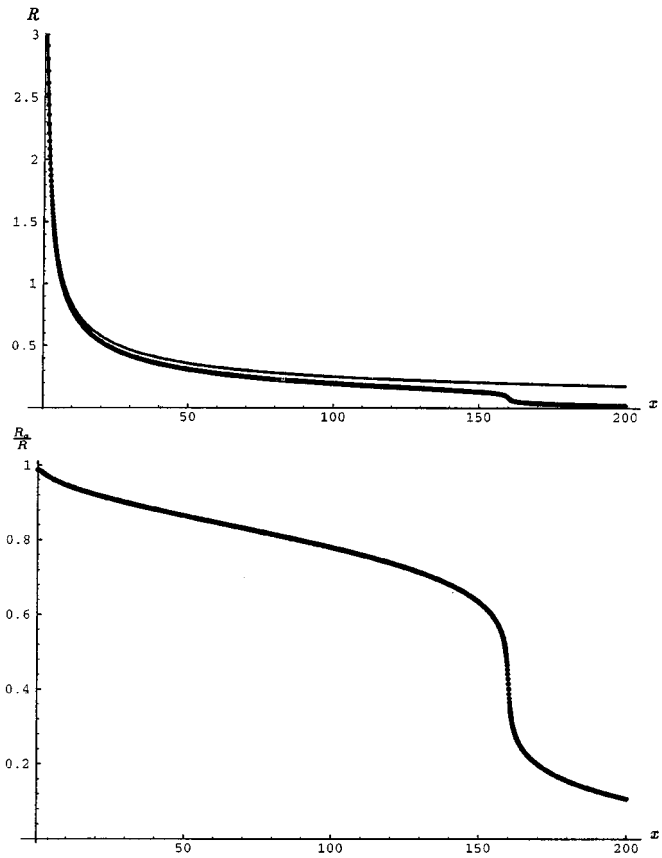

FIG. 5. Same as Fig. 4 except $r_{\max}$ is doubled to $r_{\max}=160$. The moving average method still underestimates the correlation at all scales, but the onset of the most severe underestimation occurs at this new, larger value of $r_{\max}$.

and 1600, respectively, so a very large number of terms have been kept. For $\epsilon=\frac{3}{2}$, the true covariance has a long tail and the moving average method, even with the extremely expensive resolution parameters given in Figs. 4 and 5, significantly underpredicts this long range velocity correlation. For example, the higher resolution case with $r_{\max}=160$ still fails to capture over 22% of the energy of the true velocity spectrum which resides in the region $x>160$.

How will the above behavior effect Monte Carlo simulation for the mean square displacements with $\epsilon=\frac{3}{2}$? Looking back at the second equality in (12), Figs. 4 and 5 suggest that the moving average method will necessarily significantly underpredict the mean square displacements and perhaps even give fictitious scaling exponents. The results presented in Fig. 6 of a direct Monte Carlo simulation of mean square displacement with the moving average method for the parameter choices $\overline{w}=1$, $\alpha=1$, $r_{\max}=80$, $\Delta r=0.1$, $\Delta t=0.1$, and $N=2000$ realizations confirm this. As is evident in Fig. 6, a well-defined scaling exponent emerges for the simulation utilizing the moving average method with the extremely large number of 1600 quadrature points per time step; however, this scaling exponent when compared to the exact results is clearly an artifact of the numerical procedure.

On the other hand, the moving average method performs much better than the Fourier method with comparable labor in the regime $\epsilon=\frac{1}{2}$ depicted earlier in Figs. 2 and 3. Furthermore, the conventional Fourier method performs even worse than depicted in Figs. 2 and 3 for the superdiffusive case with $\epsilon=\frac{3}{2}$ where periodicity effects are even more pronounced. Lack of space prevents a detailed description of these additional results and the interested reader can consult Ref. 20.

The above examples point out in an unambiguous fashion, through exactly solvable model problems and careful idealized numerical experiments, some of the subtleties in standard numerical procedures for Monte Carlo simulation for turbulent tracers when long range correlations occur in the velocity field. In the next section we discuss Monte Carlo simulations for fractal random fields.

III. PAIR DISPERSION STATISTICS SPANNING MANY DECADES FOR FRACTAL RANDOM FIELDS

Here we describe some new methods[6,7,10,21] for generating fractal random fields over many decades of scaling. At the end of this section we apply these methods to obtain new results on tracer pair dispersion statistics [see (6) and (7)

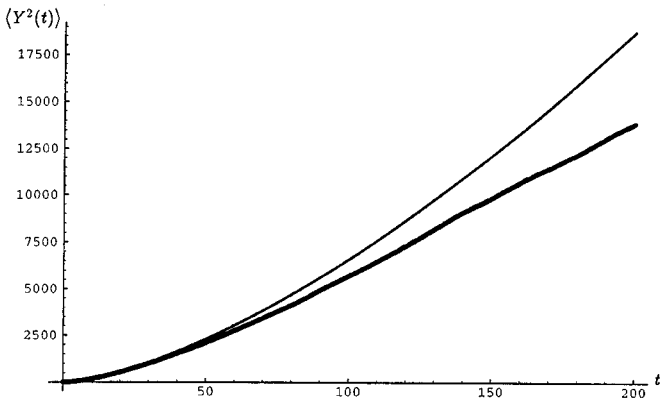

FIG. 6. Moving average method simulation results (thicker line) for $\epsilon=\frac{3}{2}$ and $r_{\max}=80$ versus the true value from (16) (thinner line). The moving average method produces an artificial scaling behavior below the true value.

above] with anisotropic incompressible random velocity fields having the Kolmogorov spectrum in two space dimensions.

A. Hierarchical Monte Carlo methods for fractal random fields

We begin by discussing Monte Carlo methods for approximating a scalar Gaussian fractal random field, $v(x)$, in a single space variable. Such a Gaussian random field is uniquely characterized up to a constant multiple by the conditions

$$\langle v(x)\rangle = 0, \qquad \langle |v(x+x')-v(x')|^2\rangle = |x|^{2H}, \tag{31}$$

where H is the Hurst exponent with $0<H<1$.[4] It is well known that almost every realization of such a field is a fractal self-similar nowhere differentiable function[4] and the exponent $H=\frac{1}{3}$ corresponds to the Kolmogorov spectrum. Such a fractal random field admits the moving average representation

$$v(x)=\int |x-y|^{H-1/2}\, dW(y), \tag{32}$$

where $dW(y)$ is Gaussian white noise.

How can we build an efficient numerical method for the fractal fields satisfying (31) which represents these fields economically over many decades? The answer is to use a hierarchical method which exploits the scaling features in (31) in a judicious fashion.[6,7,10,21] The first step is to use the moving average representation in (32) and then to localize the exact formulas very efficiently. The second step is an exact result involving expansion of white noise by a general L^2-orthonormal basis, i.e., if $\{\psi_k(y)\}_{k=1}^{\infty}$ is a complete orthonormal basis for $L^2(R)$, then

$$dW(y)=\sum_k \psi_k(y) N_k, \tag{33}$$

where N_k are standard independent identically distributed Gaussian random variables with mean zero and variance one. Inserting (33) into (32), we obtain the identity

$$v(x)=\sum_k N_k \int |x-y|^{H-1/2}\psi_k(y)\,dy. \tag{34}$$

To obtain a general hierarchical method which yields an exact representation of $v(x)$, we choose the orthonormal basis in the hierarchical form[6]

$$\psi_k(y)=\phi_{mn}^{\sigma\tau}=2^{m/2}\phi^{\sigma\tau}(2^m y-n), \tag{35}$$

where m and n are arbitrary integers and $\{\phi^{\sigma\tau}(y)\}_{\sigma=1}^{\tau}$ is a fixed finite set of functions. By inserting the functions in (35) into (34), we obtain the general exact hierarchical expansion

$$v(x)=\sum_{m=-\infty}^{\infty} \tilde{v}_m(2^m x)2^{-mH} \tag{36}$$

with

$$\tilde{v}_m(x)=\sum_{n=-\infty}^{\infty}\sum_{\sigma=1}^{\tau} G^{\sigma\tau}(x-n)N_{mn}^{\sigma\tau} \tag{37}$$

and $\{G^{\sigma\tau}(x)\}$ is the finite family of explicit functions given by

$$G^{\sigma\tau}(x)=\int_{-\infty}^{\infty}|x-y|^{H-1/2}\phi^{\sigma\tau}(y)\,dy. \tag{38}$$

for $\sigma=1,\ldots,\tau$. The representation of the stationary fractal random field $v(x)$ through the hierarchical method described in (36)–(38) is exact for any choice of a complete orthonormal basis for $L^2(R)$ defined through $\{\phi_{mn}^{\sigma\tau}\}$ from (35).

In order to convert the hierarchical expansion in (36)–(38) into a practical efficient numerical method, it is obviously important to pick functions $\{\phi^{\sigma\tau}(y)\}_{\sigma=1}^{\tau}$ to localize the convolutions $G^{\sigma\tau}(x)$ in (38) while still having $\{\phi_{mn}^{\sigma\tau}\}$ from (35) generate a complete orthonormal basis for $L^2(R)$. The way to achieve this is developed in detail in Ref. 6 where the Alpert–Rokhlin multiwavelet basis is utilized. The Alpert–Rokhlin multiwavelet

$$\{\phi^{\sigma\tau}|\sigma=1,2,\ldots,\tau\}$$

is a set of τ functions which are supported on the interval $[0, 1]$, are piecewise polynomial on $[0, \frac{1}{2}]$ and on $[\frac{1}{2}, 1]$, and satisfy the moment cancellation conditions

$$\int_{-\infty}^{\infty} x^p \phi^{\sigma\tau}(x)\,dx=0, \quad p=0,1,\ldots,\tau-1. \tag{39}$$

In addition, the set of functions $\{\phi_{mn}^{\sigma\tau}\}$ defined in (35) by translation and scaling are a complete orthonormal basis for $L^2(R)$. A concise summary of the Alpert–Rokhlin wavelets including explicit formulas is presented in Ref. 6. Clearly, the moment cancelation property in (39) for a large enough value of τ guarantees that $G^{\sigma\tau}(x)$ from (38) is highly localized so that the sum over the translates n in (37) for a fixed octave m converges rapidly.

In practical contexts, the value $\tau=4$ is sufficient for accurate simulation for the Hurst exponent $H=\frac{1}{3}$ corresponding

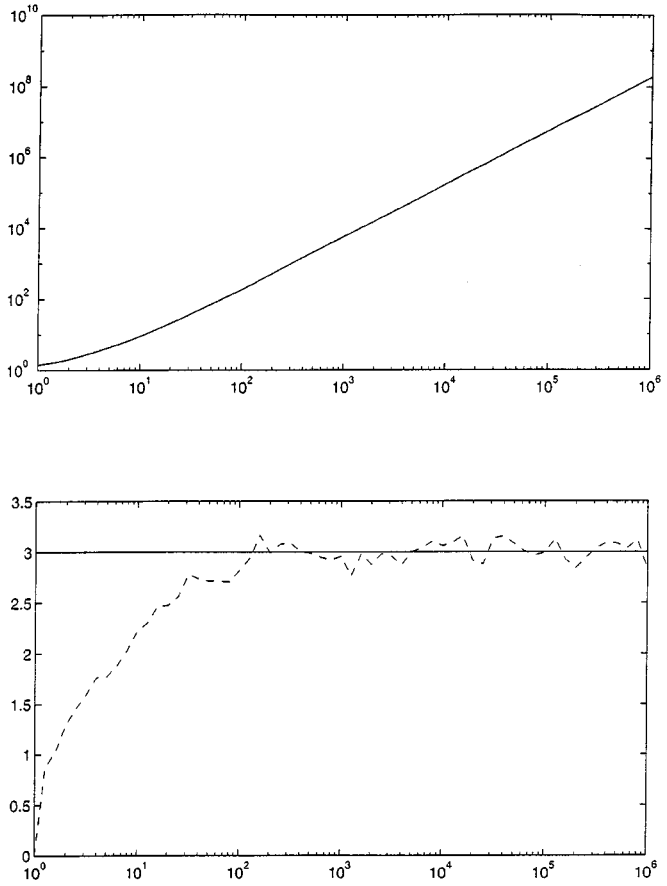

FIG. 7. The top plot contains the root mean square dispersion from an $M=2$ direction simulation using the multiwavelet algorithm. The bottom plot shows the logarithmic derivative of the rms dispersion and achieves the Richardson value of 3 over several temporal decades.

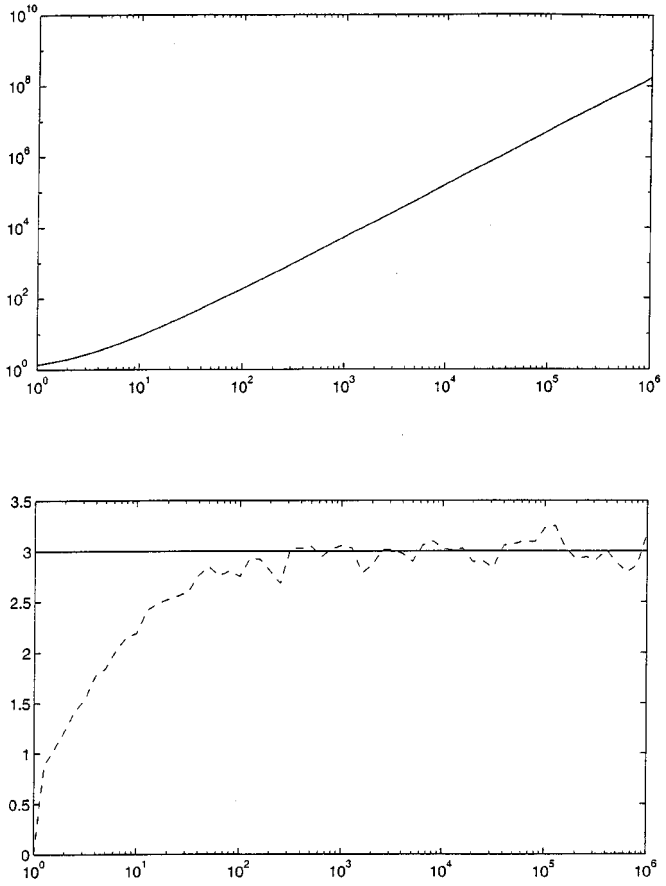

FIG. 8. Same as Fig. 7 except $M=4$ directions were used in this simulation. Again, the Richardson t^3 law is observed over several temporal decades.

to the Kolmogorov spectrum. In practice, we limit the algorithm in (36)–(38) to a finite number of scales M, and we limit the translates $\phi_{mn}^{\sigma\tau}$ to those with support within a fixed distance b from x through rigorous energy criteria. Through these judicious choices, properties such as stationarity of the field are very nearly preserved. The resulting hierarchical algorithm is given by

$$v(x)=\sum_{m=0}^{M-1}\tilde{v}_m^b(2^m x)2^{-mH} \tag{40}$$

with

$$\tilde{v}_m^b(x)=\sum_{\sigma=1}^{r}\sum_{n=\lfloor x\rfloor-b}^{\lfloor x\rfloor+b}G^{\sigma\tau}(x-n)N_{mn}^{\sigma\tau}. \tag{41}$$

The methods just described allow accurate simulation of a fractal field over 12 to 15 decades of scaling[6,7,10,21] while conventional Fourier-based methods allow accurate simulation over roughly two decades.[18] Recently, the authors have developed another more flexible alternative algorithm using wavelets in Fourier space rather than physical space.[22] A popular method in the physics community for generating such fractal random fields is the algorithm called ''successive random addition,'' SRA.[4,5] Recent work by the present authors demonstrates with full mathematical rigor that SRA cannot generate approximations consistent with a stationary Gaussian fractal field with errors necessarily scattering in the 40%–50% range for the preconstant despite the popularity of these algorithms in the physics community. On the other hand, the above multiwavelet algorithms do not suffer from this defect.[6,7,21]

As noted by two of the authors in Ref. 7, algorithms for the scalar field as described above readily generalize to vector random fields $\mathbf{v}(\mathbf{x})$ characterized by the requirements

$$\begin{aligned}&\operatorname{div}\mathbf{v}=0,\quad \langle\mathbf{v}\rangle=0,\\ &\left\langle\left([v(\mathbf{x}+\mathbf{x}')-v(\mathbf{x}')]\cdot\frac{\mathbf{x}}{|\mathbf{x}'|}\right)^2\right\rangle=|\mathbf{x}|^{2H}.\end{aligned} \tag{42}$$

This random field in (42) is the limit as $M\to\infty$ of the plane wave approximations

$$\mathbf{v}_M(\mathbf{x})=\left(\frac{\pi}{MC(H)}\right)^{1/2}\sum_{j=0}^{M-1}v_j\left[\mathbf{x}\cdot\mathbf{u}\left(\frac{\pi j}{M}\right)\right]\mathbf{u}\left[\pi\left(\frac{j}{M}+\frac{1}{2}\right)\right], \tag{43}$$

where $\mathbf{u}(\theta)=\cos\theta\ \mathbf{e}_1+\sin\theta\ \mathbf{e}_2$ and $v_j(x)$ for $j=0,\ldots,M$ are independent scalar one-dimensional fractal Gaussian random fields satisfying (31). If we select the constant $C(H)$ in (43) so that

TABLE II. Summary of the effect of anisotropy in the velocity field on the mean square dispersion (44) along various angles. Richardson's t^3 law is shown to hold with a coefficient β ranging from 0.029 to 0.032.

Number of shear fields	Angle of mean field	Beta mean	Beta min.	Beta max.	Gamma mean	Gamma min.	Gamma max.
2	45.000	0.0305	0.0269	0.0334	3.01	2.80	3.21
2	39.375	0.0311	0.0282	0.0342	3.00	2.67	3.27
2	33.750	0.0322	0.0306	0.0345	3.00	2.83	3.27
2	28.125	0.0311	0.0293	0.0326	3.00	2.75	3.21
2	22.500	0.0298	0.0287	0.0309	3.00	2.84	3.11
2	16.875	0.0311	0.0281	0.0345	3.02	2.68	3.30
2	11.250	0.0323	0.0293	0.0352	3.00	2.76	3.16
2	5.625	0.0299	0.0281	0.0317	2.99	2.72	3.16
4	45.000	0.0305	0.0269	0.0337	3.00	2.76	3.19
4	39.375	0.0326	0.0284	0.0394	3.03	2.80	3.21
4	33.750	0.0293	0.0269	0.0325	2.99	2.78	3.25
4	28.125	0.0303	0.0264	0.0345	3.00	2.69	3.19
4	22.500	0.0311	0.0277	0.0356	3.00	2.70	3.23
4	16.875	0.0303	0.0264	0.0345	3.00	2.69	3.19
4	11.250	0.0293	0.0269	0.0325	2.99	2.78	3.25
4	5.625	0.0326	0.0284	0.0394	3.03	2.80	3.21
4	0.000	0.0305	0.0269	0.0337	3.00	2.76	3.19

$$C(H)=\frac{\Gamma(\frac{1}{2})\Gamma(H+\frac{1}{2})}{2(H+1)\Gamma(H+1)}, \tag{44}$$

then as $M\to\infty$, the plane wave field in (43) converges to the isotropic incompressible fractal field with the normalization in (42). Detailed analysis[7] shows that $M=16$ already generates an isotropic field within errors of a few percent. The main point of the approximation in (43) is that scalar one-dimensional fractal random fields can be used as building blocks to synthesize multidimensional vector-valued fractal random fields so that an efficient algorithm for the scalar field automatically carries over to the multidimensional case. This is the approach utilized by two of the authors in Refs. 7 and 10 with the algorithm described in (36)–(38).

B. Application to pair dispersion with an anisotropic Kolmogorov spectrum

Here we utilize the formula in (43) together with the one-dimensional scalar multiwavelet algorithm described in (32)–(41) to build systematic anisotropic incompressible fractal fields with the low values of $M=2,4$ with the Kolmogorov value $H=\frac{1}{3}$. Such fields satisfying 12 to 15 decades of Kolmogorov scaling are constructed numerically by following the same procedure as developed earlier by the authors.[6,7,10]

We consider these anisotropic fractal fields with a large scale sweep added[10] to introduce decorrelation as in Taylor's hypothesis, i.e., we consider the fractal velocity fields $\mathbf{v}(\mathbf{x}+\mathbf{w}t)$. We compute the pair separation statistics of two tracers moving in the anisotropic fractal random field described above. Specifically, we focus on the pair dispersion defined in (6) and the preconstant in Richardson's law from (7) as a function of the anisotropy with $M=2,4$. We use the same nondimensionalization and time stepping procedure described in detail in Ref. 10 so that $|\mathbf{w}|=1$ and an initial separation distance $s=10^{-12}$. We remark that as in Sec. II such an algorithm for pair dispersion has been validated against exact solutions for $M=1$.[6] We will find that Richardson's t^3 law from (7) is valid over many decades of separation and the preconstant G_Δ is also nearly universal over many decades independent of the anisotropy in the field.

We applied the above algorithm to compute pair dispersion statistics in the scaling form

$$\sigma^2(t,s)=\beta t^\gamma, \quad t\gg 1. \tag{45}$$

Since the fields with $M=2,4$ are highly anisotropic, we varied the angle between the large scale sweep, $\mathbf{w}$, and the x_1-coordinate axis to explore the effects of anisotropy while the two particles were placed initially along the x_1 axis.

In Figs. 7 and 8, we graph the rms dispersion and the logarithmic derivative of the pair dispersion for Monte Carlo simulations averaging over 1024 realizations with $M=2$ in Fig. 7 and $M=4$ in Fig. 8 with a mean field angle of 11.25° in both cases. The graphs of the rms dispersion give a clear power law scaling regime for pair dispersion over six decades of pair separation while the logarithmic derivative test in Figs. 7 and 8 confirms Richardson's t^3 scaling law over many decades. We note that the logarithmic derivative test for scaling is a much more stringent test than the standard approach of seeking a power law fit through a least squares procedure. To determine the preconstant G_Δ, as in Ref. 10, as a stringent test we divided the computed value of $\sigma^2(t,s)$ by t^3 and determined the range for $10^3\leqslant t\leqslant 10^6$. The data for these two runs as well as other Monte Carlo simulations where we varied the number of shear directions and the mean flow angle is summarized in Table II. This table includes both the value of the exponent γ and the preconstant β from (44) as well as their scatter according to the stringent criteria described above.

As the reader can see, Richardson's t^3 law for pair separation is confirmed over many decades of pair separation even with our stringent criteria for data analysis. Further-

more, the mean of the preconstant, β, varies only from the largest values such as 0.032 to the smallest value 0.029 in all the anisotropic cases simulated. On the other hand, the simulations with isotropic fractal velocity fields with the Kolmogorov spectrum[10] with the same consistent nondimensionalization from (42) and (43) give a preconstant $\beta=0.031$ over eight decades of pair separation. The results presented here for pair separation with anisotropic Gaussian random fields give strong evidence that the preconstant G_Δ from (7) in Richardson's law is universal for Gaussian fractal fields independent of whether they are isotropic or anisotropic, although the adjustment time to achieve this scaling regime can vary with the degree of anisotropy.

ACKNOWLEDGMENTS

Andrew J. Majda's research is partially supported by grants from the National Science Foundation (NSF No. DMS-9596102-001), the Army Research Office (ARO No. DAAHO4-95-1-0345), and the Office of Naval Research (ONR No. N00014-96-1-0043). David J. Horntrop and Frank W. Elliott, Jr. were supported as postdoctoral researchers by grants from the Army Research Office and the National Science Foundation, respectively. The calculations in Sec. III of this paper were performed on the T3D at the Pittsburgh NSF Computing Center.

[1] G. Dagan, ''Theory of solute transport by ground water,'' Annu. Rev. Fluid Mech. **19**, 183 (1987).
[2] M. Lesieur, *Turbulence in Fluids* (Kluwer, Boston, 1990).
[3] G. Csanady, *Turbulent Diffusion in the Environment* (Reidel, Dordrecht, Holland, 1973).
[4] J. Feder, *Fractals* (Plenum, New York, 1988).
[5] R. Voss, ''Random fractal forgeries,'' in *Fundamental Algorithms for Computer Graphics*, edited by R. Earnshaw (Springer-Verlag, Berlin, 1985).
[6] F. Elliott and A. Majda, ''A wavelet Monte Carlo method for turbulent diffusion with many spatial scales,'' J. Comput. Phys. **113**, 82 (1994).
[7] F. Elliott and A. Majda, ''A new algorithm with plane waves and wavelets for random advection diffusion,'' J. Comput. Phys. **117**, 146 (1995).
[8] L. Richardson, ''Atmospheric diffusion shown on a distance-neighbor graph,'' Proc. R. Soc. London Ser. A **110**, 709 (1926).
[9] V. Tartarski, ''Radiophysical methods of investigating atmospheric turbulence,'' Izv. Vyssh. Ucheb. Zaved. 3 Radiofiz. **4**, 551 (1960).
[10] F. Elliott and A. Majda, ''Pair dispersion over an inertial range spanning many decades,'' Phys. Fluids **8**, 1052 (1996).
[11] D. Horntrop and A. Majda, ''Subtle statistical behavior in simple models for random advection diffusion,'' J. Math. Sci. Univ. Tokyo **1**, 23 (1994).
[12] G. Matheron and G. de Marsily, ''Is transport in porous media always diffusive? a counterexample,'' Water Resour. Res. **16**, 901 (1980).
[13] M. Avellaneda and A. Majda, ''Mathematical models with exact renormalization for turbulent transport,'' Comm. Math. Phys. **131**, 381 (1990).
[14] M. Avellaneda and A. Majda, ''Mathematical models with exact renormalization for turbulent transport II: non-Gaussian statistics, fractal interfaces, and the sweeping effect,'' Comm. Math. Phys. **146**, 139 (1992).
[15] M. Avellaneda and A. Majda, ''Simple examples with features of renormalization for turbulent transport,'' Philos. Trans. R. Soc. Ser. A **346**, 205 (1994).
[16] J. Bouchaud, A. Georges, J. Koplik, A. Provata, and S. Redner, Phys. Rev. Lett. **64**, 2503 (1990).
[17] R. Zumofen, J. Klafter, and A. Blumen, J. Stat. Phys. **65**, 991 (1991).
[18] J. Viecelli and F. Canfield, ''Functional representation of power-law random fields and time series,'' J. Comput. Phys. **95**, 29 (1991).
[19] K. Sabelfeld, *Monte Carlo Methods* (Springer-Verlag, New York, 1991).
[20] D. Horntrop, Ph.D. thesis, Program in Applied and Computational Mathematics, Princeton University, 1995.
[21] F. Elliott, A. Majda, D. Horntrop, and R. McLaughlin, ''Hierarchical Monte Carlo methods for fractal random fields,'' J. Stat. Phys. **81**, 717 (1995).
[22] F. Elliott, D. Horntrop, and A. Majda, ''A Fourier-wavelet Monte Carlo method for fractal random fields,'' to appear in J. Comput. Phys.